ISBN: 978-628-95207-4-3. ISSN: 2414-6390. Digital Object Identifier: 10.18687/LACCEI2023.1.1.883

An implementation of a system that emulates the operation of a pipe positioning arm for Raise Boring application.

Gabriel Franco[1], Oscar Jauregui[2], Leonardo Vinces, Mg[3] José Oliden, Mg[4]
[1,2,3,4] Universidad Peruana de Ciencias Aplicadas, Peru, u201718405@upc.pe, u201717144@upc.pe, leonardo.vinces@upc.pe, pceljoli@upc.edu.pe

Abstract–The lack of an automated system for pipe positioning in Raise Boring mining works (RB) generates a longer working time and higher expenses for mining companies due to a greater number of usage errors produced by the operators. Therefore, reducing the intervention of the user in the RB tunneling and raising processes is expected to increase work efficiency. The objective of the project is to design and test, through the implementation of a scale model, a pipe positioning system that operates autonomously using direct and inverse kinematics to reduce the number of people involved in the working process to carry out the same job. The function of the system is to pick up a horizontal tube and place it at the required point in a vertical position or with up to a 45° inclination with a 4 degrees of freedom (DOFs) robotic arm. The implementation was made with servo motors, and the parts were printed in 3D using PLA. The coordinates of the arm positions were obtained through simulations carried out in Python code, which were compared with the resulting coordinates of the prototype implementation. After that, an accuracy of 96.29% and an average operation time of 16.21 seconds were obtained in the tests carried out with the prototype, demonstrating the effectiveness of the implemented system.

Keywords-- servomotor, pipe positioner, raise boring, automation, kinematics, raspberry pi

I. Introduction

Due to the increasing number of mining projects in Peru and the region, there is a growing urgency to optimize the efficiency of drilling machines and related equipment in order to generate the maximum economic income for companies. Raise Boring machines are among the fastest, safest, and most efficient machines used for drilling, tunneling, and chimney work, as they can create vertical or inclined holes and connect different levels at varying heights [1]. However, to manipulate pieces and extract material, access to both levels is necessary. A pilot hole is first created from the upper to the lower level with a diameter of about 230-350mm, and once the levels are connected, a reamer with a larger diameter is used to enlarge the hole, allowing the material to fall to the lower level due to gravity [2-4].

To locate the position of the arm claw, the kinematic analysis of the system was carried out using measurements from the prototype. Kinematic calculations can be divided into two types: forward and inverse kinematics. Forward kinematics calculate the position and orientation of the end effector from the given joint variables [5], while inverse kinematics calculate the set of joint angles required for the robot to achieve the desired position. To obtain the points of interest, a geometric method was chosen [6,7], and the Denavit-Hartenberg method was used for forward kinematics, while the inverse kinematic model was found from the homogeneous transformation matrix.

Raheem et al [8] designed a robotic arm using inverse kinematics and the ANFIS model to teach children how to write in schools. With this project, they obtained a maximum error of approximately 1.6 cm in each axis, due to the commercial servo motors used. However, the fuzzy logic models used for the control consume a lot of computational loads, so this type of control was not used for this work.

My et al [9] designed an automated control system for a 6 DOF welding robot incorporated with a rotary positioner to optimize the 3D welding process, managing to minimize the kinematic error to 0.001mm of deviation from the proposed route. However, the authors did not carry out a mechanical implementation to validate their results in the field, so there are no real results of the equipment behavior.

Suarez et al [10] developed a lightweight robotic system with a double arm, capable of lifting pieces of up to 750g with 5 DOFs per arm driven by servo motors, to be placed in unmanned vehicles and serve in high-altitude and high-hazard work. The structure of the control system is based on inverse kinematics. However, the arm does not have the ability to lift objects, and its speed has been limited to avoid the same problem.

The results of the simulations were verified in the experimental tests of the prototype. The comparison between the results of the simulated model and the experimental model shows that the implemented scale model of the pipe positioning arm meets the proposed objectives of the project, paving the way for the development of the real model of the pipe positioning arm to operate in Raise Boring type mining works in the future.

II. SYSTEM DESCRIPTION

The implemented system emulates the operation and control methodology of a conventional Raise Boring positioner arm machinery. However, it has the added feature of an automatic control mode for the execution of the pipe positioning and removal process. The main objective of this system is to validate the established logic and potentially adapt it to a real

Digital Object Identifier: (only for full papers, inserted by LACCEI).
ISSN, ISBN: (to be inserted by LACCEI).
DO NOT REMOVE

size model. The diagram of the operation and control system of the model is shown in *Fig. 1* and is detailed in next paragraphs.

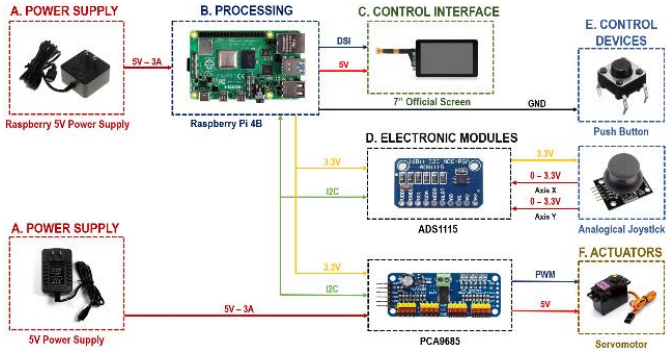

Fig. 1. System block diagram

A. *Power Supply*

The power supply of the system is given by two 5VDC sources. The first source model KSA-15E-051300HU of the Raspberry Pi brand corresponds to the power supply of the processing section of the system, while the second source model XBS-0530 corresponds to the power supply of the electronic modules section, more precisely to the PCA9685 module.

B. *Processing*

For the development of the proposed system, a Raspberry Pi 4B board was utilized, which is responsible for data processing and commanding the actuators by applying the operating logic established through Python programming. Additionally, the Raspberry Pi acts as the master device for communication of the electronic modules via the I2C communication bus.

C. *Control Interface*

For the project implementation, a human-machine interface (HMI) was designed to control the system and display real-time configuration data and arm coordinates. To achieve this, a 7-inch touch screen model 7Touch from the Raspberry Pi brand was integrated, and a visual interface was developed using the Tkinter library in Python programming.

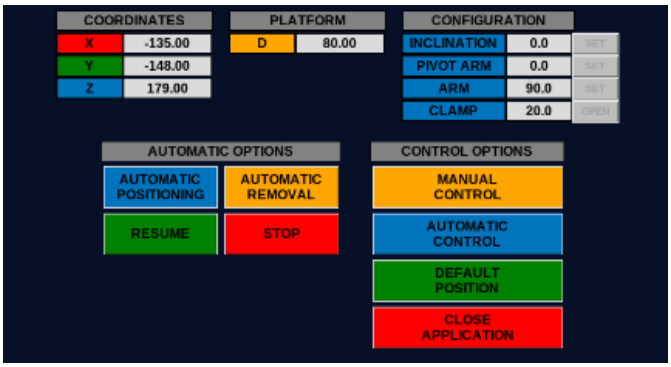

Fig. 2. Control interface main screen

As it can be seen in the main screen of the interface shown in *Fig. 2*, the interface offers different control options. Among the main ones is the manual control option, which enables the control of the system through the control devices, and at the same time, provides manual configuration options of the angle of each of the servo motors through a panel where the value of the desired angle is entered.

In the same way, there is an automatic control option within the control options. This mode will disable the manual control mode, and it will be possible to execute the pipe positioning or removal operations, depending on the one selected. This option will also allow you to stop or resume the execution of the operation.

Finally, there is the default position option, which will return the arm configuration to its initial state, and the close application option, which will return the arm to its initial state and close the application.

D. *Electronic Modules*

Due to the functionality established for the system, it was necessary to acquire certain electronic modules corresponding to the digital analog conversion of electrical signals and the command of servomotors by pulse width modulation (PWM) signals.

ADS1115 module: Due to the limitation of not having analog inputs on the Raspberry Pi board, it was necessary to acquire an analog to digital signal converter (ADC) module.

PCA9685 module: It is known that the Raspberry Pi board can send PWM signals, however, it only can generate two PWM signals simultaneously, which is why it was necessary to acquire a servomotor controller module.

Both modules make use of the I2C bus of the Raspberry Pi in order to send and receive data.

E. *Control Devices*

The mechanism of this system is controlled using an analog joystick with two axes and three buttons. The analog joystick is utilized to control the movement of the positioning arm rotation axes in proportion to the movement of the joystick. Additionally, two buttons are used to activate the opening or closing of the claw of the arm. Finally, the remaining button serves the function of enabling the control of the positioning arm through the joystick and the claw buttons. This is done as a safety measure to prevent inadvertent actuation of the arm and thus mitigate potential risks.

F. *Actuators*

To activate the rotary movements of the arm mechanism, four servomotors are used, which were selected according to the necessary torque. The specific models of servomotors used are the MG996R, MG996, and SG90.

III. ELECTRICAL SCHEMATIC

An electrical wiring diagram was created using the Eplan Education 2022 software based on the block diagram shown in Fig. 1 and the specifications provided in the data sheets of each system component. *Fig. 3* displays the electrical schematic of the system and illustrates the interconnections between the components described in Section II, System Description.

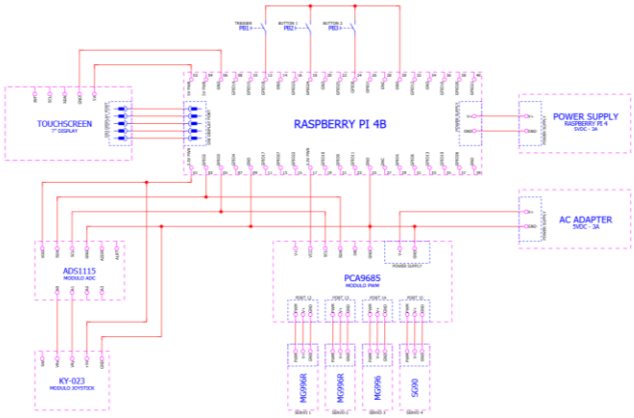

Fig. 3. System electrical schematic

III. MECHANICAL DESIGN

For the project to fulfill the function of collecting and positioning pipes, the arm was required to overcome certain mechanical restrictions of the servomotors, selected materials, friction between components, dimensions, temperature, etc. *Fig. 4* shows the block diagram of the mechanical design and the relation between each component with the rest of them.

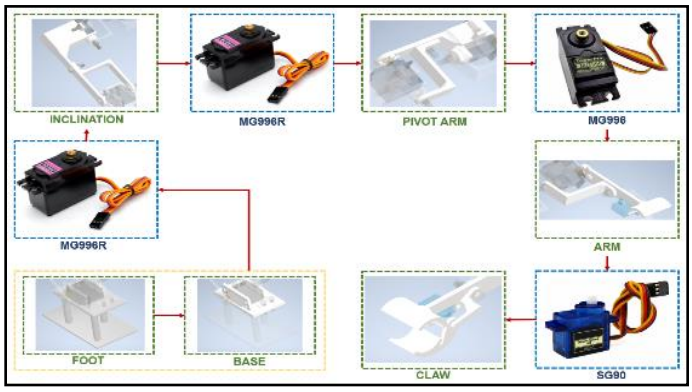

Fig. 4. Mechanical design block diagram

A. Design Considerations

1) Actuators: The servomotors mentioned in section 2.F were selected for their ability to provide enough torque to support the mechanical structure of the arm and maintain a constant speed throughout its range of motion. The three different models were strategically placed in the positions shown in *Fig. 4.*

MG996R: Of the three models used, the MG996R is the strongest servo motor and provides a torque of around 10 Kg·cm at 5V. This model was chosen to be placed on the Base since it needs to support the entire weight of the mechanism. It was also placed on the Arm because it is the only one that maintains a constant speed at any point of the range of motion.

MG996: It is a servomotor with a force and size similar to the previous model. It provides a torque of approximately 8 Kg·cm at 5V. This model was used on the Pivot arm because it has the same dimensions as the previous model, which makes it easier to design the supporting components. Additionally, it offers lower torque, making it more cost-effective. It can maintain a constant speed at any required point.

SG90: It is a smaller servo motor and offers less torque. Its torque is approximately 1.5 Kg·cm at 5V. and it is located at the end of the mechanism, on the Inclination arm, with the sole purpose of opening and closing the Claw, so this servomotor is not required to have greater torque.

2) Materials: Two different materials were used for implementing the parts.

PLA: Filament of this material was chosen for 3D printed parts as it has the best balance between mechanical properties and cost [11-13]. Parts were printed at a 20% density setting.

Iron: It was used for fabricating the Foot due to its density of approximately 7.8 g/cm3, which provides greater weight and stability to the mechanism. It can also withstand the deformation exerted by the mechanism.

B. 3D Modeling

The 3D model of the mechanism can be seen in *Fig. 5*. It consists of 13 support pieces adapted to the dimensions of each servomotor held by 14 3/16” bolts and nuts. Following the position of the parts of the mechanical design block diagram shown in *Fig. 4*, all the parts, except for the Foot, are 3D printed with PLA.

In addition, the 3 black servomotors are the MG996R and MG996. The 2 servomotors closest to the base correspond to the first model, and the second model to the furthest from the base, on the Pivot arm. Finally, the blue servomotor, the SG90, is on the far right, near the Claw.

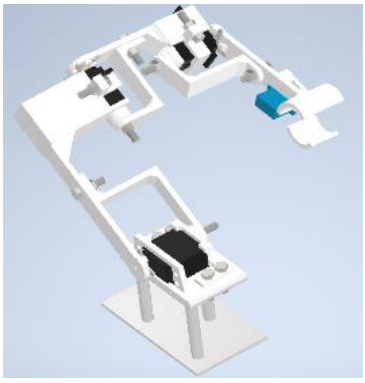

Fig. 5. 3D Model of the mechanism

C. Implementation

The implementation took into account the considerations developed in the previous section. *Fig. 6* shows an image of the implemented model. In this way, it can be seen that the Foot is the gray-colored piece, and the 12 white pieces are the ones printed with PLA, joined by screws and nuts, while the actuators are among the support pieces.

Fig. 6. Real model of the pipe positioner arm

IV. KINEMATIC CALCULATIONS

The automation of the proposed system is based on studies of forward and inverse kinematics for analyzing the movement of robotic mechanisms. These kinematic analyses aim to obtain the configuration that the arm mechanism must adopt to reach the coordinates of the points of interest that correspond to the pipe collection point and the positioning point.

To find the forward kinematics of the arm, the Denavit-Hartenberg (DH) representation was applied. The inverse kinematic model is obtained from the homogeneous transformation matrix that was derived from the forward kinematic model. Finally, by means of geometric calculations, the coordinates of the points of interest are determined. The kinematic resolutions were carried out based on what was established by Barrientos et al. [14] in their research document "*Fundamentals of Robotics*."

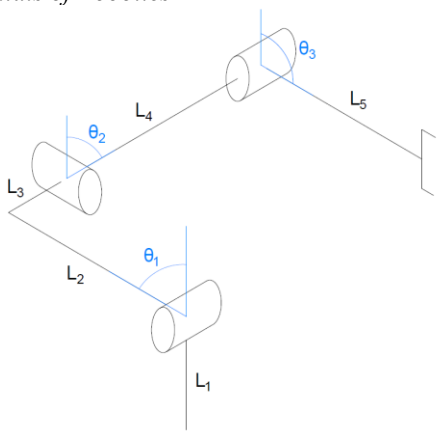

Fig. 7. Arm kinematic model

To develop the kinematic calculations, the simplified kinematic model presented in *Fig. 7* will be used as a base. In this model, the joints and lengths to be considered for the calculations are established.

A. Forward Kinematics

To apply the DH representation, the first step to follow is to find the reference axes of the mechanism (According to *Fig. 7*) using only the X and Z axes for the transformations of translation and rotation between each axis. For this, the base of the arm is taken as the initial reference point, while for the last reference point the center of the gripper mechanism is considered.

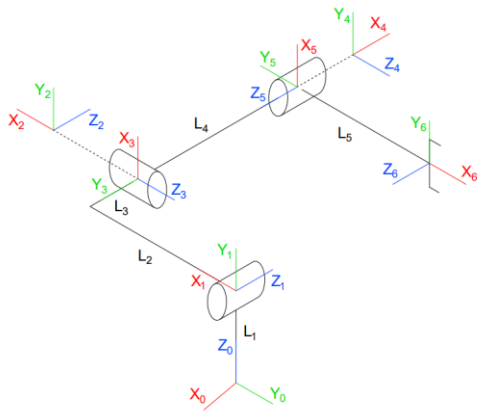

Fig. 8. Reference axes of the kinematic model

From the previously found reference axes, the table of DH parameters corresponding to the transformations of rotation and translation in the X and Z axes is made (*Tab. 1*).

The following measurements based on the previously performed mechanical implementation were considered (all in millimeters).

$$L_1 = 90 \quad L_2 = 150.5 \quad L_3 = 7.2 \quad L_4 = 130 \quad L_5 = 116.5$$

TABLE I
DENAVIT-HARTENBERG PARAMETER TABLE

A	θ_i **(Z)**	d_i **(Z)**	a_i **(X)**	α_i **(X)**
0-1	$-90°$	L_1	0	90°
1-2	θ_1	L_3	L_2	0°
2-3	90°	0	0	$-90°$
3-4	$\theta_2 - 90°$	0	L_4	0°
4-5	90°	0	0	$-90°$
5-6	$\theta_3 - 90°$	0	L_5	0

After obtaining the table of DH parameters, the transformation matrices between each axis are calculated as follows:

$$^{i-1}A_i = \begin{bmatrix} \cos\theta_i & -\cos\alpha_i \text{sen}\theta_i & \text{sen}\alpha_i \text{sen}\theta_i & a_i\cos\theta_i \\ \text{sen}\theta_i & \cos\alpha_i\cos\theta_i & -\text{sen}\alpha_i\cos\theta_i & a_i\text{sen}\theta_i \\ 0 & \text{sen}\alpha_i & \cos\alpha_i & d_i \\ 0 & 0 & 0 & 1 \end{bmatrix}$$

Finally, the homogeneous transformation matrix T is

obtained from the product of the transformation matrices ${}^{i-1}A_i$.

$$T = {}^{0}A_1 \, {}^{1}A_2 \ldots {}^{n-1}A_n$$

$$T = \begin{bmatrix} n_x & o_x & a_x & p_x \\ n_y & o_y & a_y & p_y \\ n_z & o_z & a_z & p_z \\ 0 & 0 & 0 & 1 \end{bmatrix}$$

From this matrix it is possible to obtain the Cartesian coordinates of the end point of the arm mechanism by means of the values p_x, p_y, p_z.

B. *Inverse Kinematics*

The resolution of the inverse kinematic model is calculated from the homogeneous transformation matrix obtained from the forward kinematic model. This method consists in obtaining the equations of the angular variables corresponding to the mechanism of the arm. These equations are obtained from the relationship of the equations contained in the homogeneous transformation matrix T in the following way:

$$T = {}^{0}A_1 \, {}^{1}A_2 \, {}^{2}A_3 \, {}^{3}A_4 \, {}^{4}A_5 \, {}^{5}A_6$$

$$({}^{1}A_2)^{-1}({}^{0}A_1)^{-1}T = {}^{2}A_3 \, {}^{3}A_4 \, {}^{4}A_5 \, {}^{5}A_6$$

$$\begin{bmatrix} 0 & -\cos\theta_1 & \operatorname{sen}\theta_1 & -L_2 - L_1\operatorname{sen}\theta_1 \\ 0 & \operatorname{sen}\theta_1 & \cos\theta_1 & -L_1\cos\theta_1 \\ -1 & 0 & 0 & -L_3 \\ 0 & 0 & 0 & 1 \end{bmatrix} \begin{bmatrix} n_x & o_x & a_x & p_x \\ n_y & o_y & a_y & p_y \\ n_z & o_z & a_z & p_z \\ 0 & 0 & 0 & 1 \end{bmatrix}$$

$$= \begin{bmatrix} -\cos\theta_3 & \operatorname{sen}\theta_3 & 0 & -L_5\cos\theta_3 \\ \operatorname{sen}\theta_3\cos\theta_2 & \cos\theta_2\cos\theta_3 & -\operatorname{sen}\theta_2 & L_4\operatorname{sen}\theta_2 + L_5\operatorname{sen}\theta_3\cos\theta_2 \\ -\operatorname{sen}\theta_2\operatorname{sen}\theta_3 & -\operatorname{sen}\theta_2\cos\theta_3 & -\cos\theta_2 & L_4\cos\theta_2 - L_5\operatorname{sen}\theta_2\operatorname{sen}\theta_3 \\ 0 & 0 & 0 & 1 \end{bmatrix}$$

- Selecting element (1,4):

$$-Y\cos\theta_1 + Z\operatorname{sen}\theta_1 - L_2 - L_1\operatorname{sen}\theta_1 = -L_5\cos\theta_3$$

$$L_5\cos\theta_3 = Y\cos\theta_1 - Z\operatorname{sen}\theta_1 + L_1\operatorname{sen}\theta_1 + L_2$$

$$\theta_3 = \cos^{-1}\left(\frac{Y\cos\theta_1 + (L_1 - Z)\operatorname{sen}\theta_1 + L_2}{L_5}\right) \quad (1)$$

- Selecting element (3,4):

$$-X - L_3 = L_4\cos(\theta_2) - L_5\operatorname{sen}(\theta_2)\operatorname{sen}(\theta_3)$$

$$L_5 sin(\theta_2) sin(\theta_3) = L_4 cos(\theta_2) + X + L_3$$

$$\theta_3 = sin^{-1}\left(\frac{L_4 cos(\theta_2) + X + L_3}{L_5 sin(\theta_2)}\right) \quad (2)$$

As can be seen, two equations were obtained for the value θ_3, equation (1) depending on the variable θ_1 and equation (2) on the variable θ_2. Since the value of θ_1 is known as it is a constant provided by the operator, the first equation will be used to find the value of θ_3.

In the case of θ_2. Equation (2) is used by mapping values between 0° to 90° through Python programming so that the value of θ_3 obtained from equation (1) match with that value obtained in equation (2).

C. *Interest points coordinates calculations*

The equations for the coordinates of interest points corresponding to the positioning and collecting points are obtained by means of the geometric method.

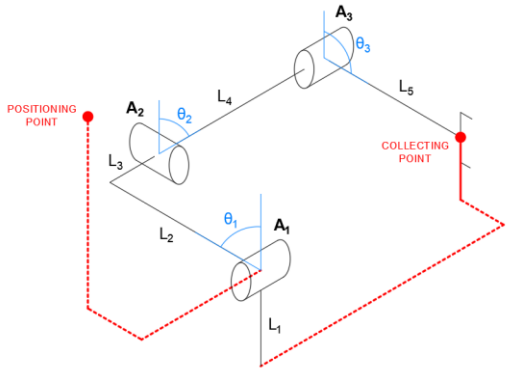

Fig. 9. Location of interest points in the kinematic model

A. *Positioning Point*

To perform the pipe positioning function in the drilling rig, joint A2 is required to have a value of $\theta_2 = 90°$.

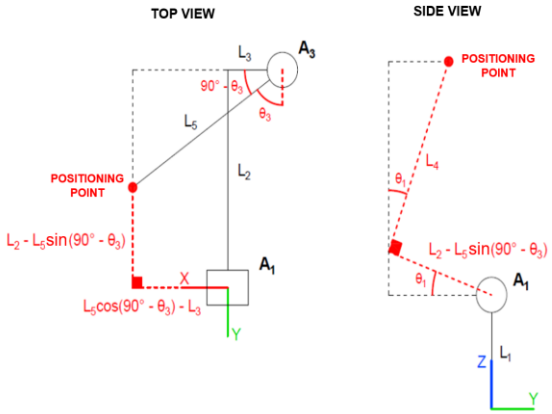

Fig. 10. Top and side view of the positioning point scope setup.

We proceed to find the equations of the coordinates of the positioning point with respect to θ_1 and considering the established coordinate axis.

$$X_{pos} = L_5 \, cos \, cos \, (90 - \theta_3) \; - L_3 \quad (3)$$

$$Y_{pos} = L_4 \, sin \, sin \, (\theta_1) \; - [L_2 - L_5 \, sin \, sin \, (90 - \theta_3) \,] cos\theta_1 \quad (4)$$

$$Z_{pos} = L_1 + [L_2 - L_5 \, sin \, sin \, (90 - \theta_3) \,] sin\theta_1 + L_4 cos\theta_1 \quad (5)$$

B. Collecting Point

To perform the function of collecting pipes on the resting platform, joint A_2 is required to have an angle of $\theta_2 = 0°$.

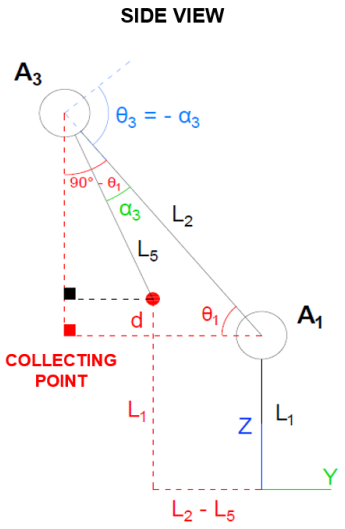

Fig. 11. Side view of the collecting point scope setup.

Due to the positioning arm mechanism, joint A3 must assume a negative angle value so that the end of the arm can reach the pick point regardless of the tilt value θ_1.

This means that the value of the Z coordinate will depend on the values θ_1 and θ_3. Since θ_1 is a constant provided by the operator, the possible values of θ_3 must be mapped so that the end of the arm can reach the collection point and thus obtain the coordinate corresponding to Z.

$$X_{col} = -L_3 - L_4 \quad (6)$$

$$Y_{col} = L_5 - L_2 \quad (7)$$

$$Z_{col} = L_1 + L_2 sin\theta_1 - L_5 \, cos \, cos \, (90 - \theta_1 + \theta_3) \quad (8)$$

Observing *Fig. 11* we can determine that:

$$L_5 - L_2 = L_5 sin(90° - \theta_1 + \theta_3) - L_2 cos\theta_1 \quad (9)$$

To obtain the value of θ_3 and to obtain the value of the Z coordinate, Python programming is used to map values between -20° to 0° of the value of θ_3 applied to equation (9), until finding the value of θ_3 that validates the equality stated in this equation.

VI. RESULTS

The following table (*Tab. 2*) compares the theoretical resulting positions of the mechanism with the resulting positions of the implemented model seen in *Fig. 6.*

All 3 angles of input data belong to the angles exposed in *Fig. 7* and four positions of interest have been chosen, of which the positioning coordinates are placed as the positions 1 and 3, and its visual representation is the *Fig. 10*. On the other hand, the collecting coordinates are placed as the positions 2 and 4 and its visual representation corresponds to *Fig. 11.*

TABLE II
RESULTS COMPARISON TABLE (MEASUREMENTS IN MM)

	INPUT DATA			THEORETICAL OUTPUT DATA			REAL OUTPUT DATA		
POS	θ_1	θ_2	θ_3	X	Y	Z	X	Y	Z
1	0°	90°	45°	75	-68	216	74	-74	222
2	0°	0°	0°	-137	-34	90	-142	-40	84
3	45°	90°	45°	75	44	230	78	47	279
4	45°	0°	0°	-137	-24	114	-145	-30	111

The values corresponding to the theoretical results were obtained by kinematic calculations, while the real coordinates were obtained by using a measuring tape on the real model.

According to the theoretical and real output data shown in *Tab. 2*, an average precision percentage of 96.29% and a maximum error of 5.84% were obtained, which is considered a favorable value for the implemented model. Additionally, the times for the execution of the positioning and collection operations were recorded, obtaining an average time of 16.21 seconds.

VII. CONCLUSIONS

This paper has presented the design of a robotic arm with 4 DOF that allows one to pick up a pipe in a horizontal position and place it in a vertical position or with the selected angle of inclination. Three DOFs allow the Claw to move from one point in space to another, and the last DOF enables the claw to open and close. The arm structure consists of 13 parts, of which 12 were 3D printed with PLA and 1 was manufactured with iron.

The kinematic model allows to properly control the mechanism and reach the desired position with a maximum error of 5.84%, which is largely due to the deformation suffered by certain parts in some positions of the mechanism, primarily the pieces printed in 3D, because of the material which it has been manufactured with or the manufacture process.

However, the control system is considered to work properly and in future works it is planned to implement the mechanism on a much larger scale to carry out real mining works.

ACKNOWLEDGMENT

To the Research Directorate of the Peruvian University of Applied Sciences for the support provided to carry out this research work UPC-EXPOST-2022-2

REFERENCES

[1] Hu, X.-K., Liu, Z.-Q., & Tan, H. (2021). Influence of engineering parameters on rock breaking performance of raise boring machine.

Measurement: Journal of the International Measurement Confederation, 174. https://doi.org/10.1016/j.measurement.2021.109005

[2] Shaterpour-Mamaghani, A., Copur, H., Dogan, E., & Erdogan, T. (2018). Development of new empirical models for performance estimation of a raise boring machine. Tunnelling and Underground Space Technology, 82, 428–441. https://doi.org/10.1016/j.tust.2018.08.056

[3] Shaterpour-Mamaghani, A., & Copur, H. (2021). Empirical Performance Prediction for Raise Boring Machines Based on Rock Properties, Pilot Hole Drilling Data and Raise Inclination. Rock Mechanics and Rock Engineering, 54(4), 1707–1730. https://doi.org/10.1007/s00603-020-02355-1

[4] Liu, Z., & Meng, Y. (2015). Key technologies of drilling process with raise boring method. Journal of Rock Mechanics and Geotechnical Engineering, 7(4), 385–394. https://doi.org/10.1016/j.jrmge.2014.12.006

[5] Shen, H., Liu, Y., Wu, H., Hu, C., & Wang, S. (2018). Forward and Inverse Kinematics for a Novel Double Scara Robot. IOP Conference Series: Earth and Environmental Science, 170(4). https://doi.org/10.1088/1755-1315/170/4/042088

[6] Singh, G., Banga, V. K., & Yingthawornsuk, T. (2019). Inverse kinematics solution of programmable universal machine for assembly (PUMA) robot. Proceedings - 15th International Conference on Signal Image Technology and Internet Based Systems, SISITS 2019, 518–524. https://doi.org/10.1109/SITIS.2019.00088.

[7] Wang, X., Yuan, D., Wang, X., & Wu, J. (2022). Kinematic Analysis and Virtual Prototype Simulation of the Thrust Mechanism for Shield Machine. Applied Sciences (Switzerland), 12(3). https://doi.org/10.3390/app12031431

[8] Raheem, F. A., Khaleel, H. Z., & Kashan, M. K. (2018). Robot Arm Design for Children Writing Ability Enhancement using Cartesian Equations based on ANFIS. 2018 3rd Scientific Conference of Electrical Engineering, SCEE 2018, 150–155. https://doi.org/10.1109/SCEE.2018.8684038

[9] My, C. A., Bien, D. X., Tung, B. H., Hieu, L. C., Cong, N. V., & Hieu, T. V. (2019). Inverse kinematic control algorithm for a welding robot-positioner system to trace a 3D complex curve. International Conference on Advanced Technologies for Communications, 2019-Octob, 319–323. https://doi.org/10.1109/ATC.2019.8924540

[10] Suarez, A., Jimenez-Cano, A. E., Vega, V. M., Heredia, G., Rodriguez-Castaño, A., & Ollero, A. (2018). Design of a lightweight dual arm system for aerial manipulation. Mechatronics, 50, 30–44. https://doi.org/10.1016/j.mechatronics.2018.01.005

[11] Mazzanti, V., Malagutti, L., & Mollica, F. (2019). FDM 3D printing of polymers containing natural fillers: A review of their mechanical properties. Polymers, 11(7). https://doi.org/10.3390/polym11071094

[12] Liu, Z., Wang, Y., Wu, B., Cui, C., Guo, Y., & Yan, C. (2019). A critical review of fused deposition modeling 3D printing technology in manufacturing polylactic acid parts. International Journal of Advanced Manufacturing Technology, 102(9–12), 2877–2889. https://doi.org/10.1007/s00170-019-03332-x

[13] Ilyas, R. A., Sapuan, S. M., Harussani, M. M., Hakimi, M. Y. A. Y., Haziq, M. Z. M., Atikah, M. S. N., Asyraf, M. R. M., Ishak, M. R., Razman, M. R., Nurazzi, N. M., Abral, H., & Asrofi, M. (2021). Polylactic acid (Pla) biocomposite: Processing, additive manufacturing and advanced applications. Polymers, 13(8). https://doi.org/10.3390/polym13081326

[14] Barrientos, A., Peñin, L., Balaguer, C., & Aracil, R. (2007). Fundamentos de Robótica. 2da Edición. McGraw-Hill/Interamericana de España S.A. http://www.upm.es/observatorio/vi/index.jsp?pageac=actividad.jsp&id_actividad=2646

[15] Menendez, E., Victores, J. G., Montero, R., Martínez, S, & Balaguer, C. (2018). Tunnel structural inspection and assessment using an autonomous robotic system. Automation in Construction, 87, 117–126. https://doi.org/10.1016/j.autcon.2017.12.

[16] R. G. V. Andrade and L. Vinces, "A Comparative Analysis of Kinematics of Industrial Robot KUKA KR 60–3 Using Scientific Computing Languages," 2020 Asia Conference on Computers and Communications (ACCC), 2020, pp. 114-119, doi: 10.1109/ACCC51160.2020.9347897.

[17] Alejandro, D., Matos, J., Vinces, L., Mirko, H. (2022). Analysis of an Automated System in a Robotized Cell for the Transport, Control, Classification, and Organization of Heterogeneous Packages. In: Iano, Y., Saotome, O., Kemper Vásquez, G.L., Cotrim Pezzuto, C., Arthur, R., Gomes de Oliveira, G. (eds) Proceedings of the 7th Brazilian Technology Symposium (BTSym'21). BTSym 2021. Smart Innovation, Systems and Technologies, vol 295. Springer, Cham. https://doi.org/10.1007/978-3-031-08545-1_45

[18] Chicoma, M.U., Escobar, D.S., Vinces, L. (2022). Large-Scale FDM 3D Printing in 6 Degrees of Freedom on One ARM KUKA KR 60. In: Iano, Y., Saotome, O., Kemper Vásquez, G.L., Cotrim Pezzuto, C., Arthur, R., Gomes de Oliveira, G. (eds) Proceedings of the 7th Brazilian Technology Symposium (BTSym'21). BTSym 2021. Smart Innovation, Systems and Technologies, vol 295. Springer, Cham. https://doi.org/10.1007/978-3-031-08545-1_53

[19] Andrade, R.G.V., Vinces, L. & Lau, K. A modular mechatronic gripper installed on the industrial robot KUKA KR 60-3 for boxing, unpacking and selecting of beverage bottles. Int J Interact Des Manuf (2022). https://doi.org/10.1007/s12008-022-00879-0

[20] Tung, T. T., van Tinh, N., Phuong Thao, D. T., & Minh, T. V. (2023). Development of a prototype 6 degree of freedom robot arm. Results in Engineering, 18, 101049. https://doi.org/10.1016/j.rineng.2023.101049

[21] Chen, F., Ju, H., & Liu, X. (2023). Inverse kinematic formula for a new class of 6R robotic arms with simple constraints. Mechanism and Machine Theory, 179, 105118. https://doi.org/10.1016/j.mechmachtheory.2022.105118

[22] Guan, D., Yang, N., Lai, J., Siu, M.-F. F., Jing, X., & Lau, C.-K. (2021). Kinematic modeling and constraint analysis for robotic excavator operations in piling construction. *Automation in Construction*, *126*, 103666. https://doi.org/10.1016/j.autcon.2021.103666